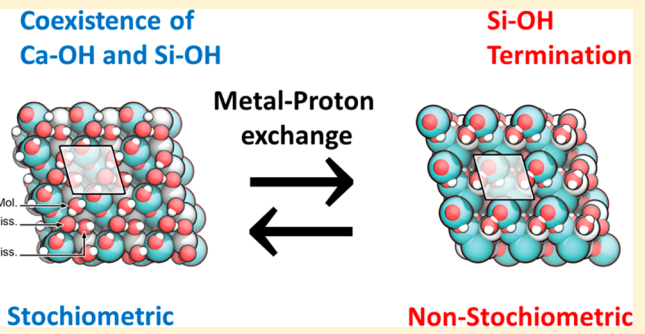


Formation of Hydroxyl Groups at Calcium-Silicate-Hydrate (C-S-H): Coexistence of Ca—OH and Si—OH on Wollastonite(001)

Simone Sanna,[†] Wolf Gero Schmidt,[†] and Peter Thissen^{*,‡}[†]Lehrstuhl für Theoretische Physik, Universität Paderborn, 33098 Paderborn, Germany[‡]Karlsruher Institut für Technologie, Institut für Funktionelle Grenzflächen, Hermann-von-Helmholtz-Platz 1, 76344 Eggenstein-Leopoldshafen, Germany

ABSTRACT: Total-energy calculations based on density-functional theory are combined with ab initio thermodynamics to better understand the pH-value-dependent water–wollastonite(001) (CaSiO_3) interaction. The truncation of wollastonite(001) is found to lead to nearly negligible ionic relaxation with respect to the bulk geometry. The thermodynamic ground state for low water coverage gives rise to a molecular adsorption energy of about 2 eV and features coexisting Si—OH and Ca—OH groups at the wollastonite(001) surface. The adsorption energy per molecule decreases to 1.4 eV with increasing the coverage to one monolayer. For water coverages in excess of one monolayer, adsorption energies close to the value characteristic for water adsorption on ice are obtained. More favorable than stoichiometric interfaces, however, are water–wollastonite(001) interfaces that are enriched in Si—OH sites: Even at basic pH values, a metal–proton exchange reaction at the water–wollastonite(001) interface lowers the total energy.



1. INTRODUCTION

Interfacial reactions between solid surfaces and aqueous solutions are important in the case of concrete, which plays a key role for today's technical infrastructure: To increase the service life of concrete, efficient and effective ways of surface functionalization that hinder corrosion are sought. Therefore, the microscopic understanding of the concrete interface formed with water is essential. Calcium-silicate-hydrate (C-S-H) phases are the basic building blocks of ordinary Portland cement.^{1,2} In general, the microstructure of hydrated cement paste, as shown on the left side of Figure 1, is characterized by two main pore

networks. The first pore network is the space in the cement paste not filled with hydration products, called the capillary pore space. The second pore network is specifically associated with the C-S-H gel phase. Pores contain adsorbed water that plays an important role in drying shrinkage and creep, and they are responsible for the extremely high surface area of C-S-H phases. The interaction of wollastonite(001) surfaces with water of varying pH value is investigated here computationally to get microscopic insight into C-S-H surfaces exposed to ambient conditions.

Wollastonite (CaSiO_3) is a fiber mineral formed by chains of Si—O tetrahedra. The structure cell contains two apex-to-apex joining tetrahedra and one tetrahedron with one edge parallel to the chain direction.³ These Si—O chains are Ca coordinated. Till now, the microscopic structure of the water–wollastonite(001) interface has not been understood. The existence of different surface atomic species opens a variety of plausible bonding scenarios with water. Thus, the termination of the surface by hydroxyl groups is of particular interest for various further surface reactions. The activation energy of these hydroxyl groups required in chemical reactions largely determines the surface chemistry.

In the present work it is shown that single water monomers adsorb dissociatively on wollastonite(001) and lead to a coexistence of Si—OH and Ca—OH groups of different

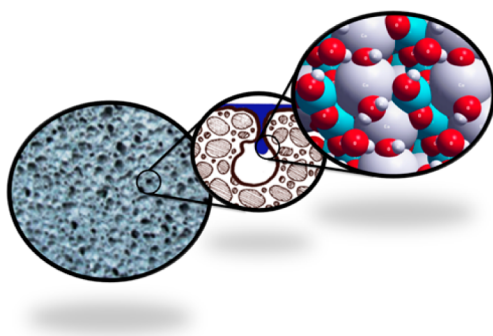


Figure 1. From left to right: Microscopic picture of the cleavage plane of Portland cement. Sketch of a side cut through a capillary pore, half-filled with water. Top view on an atomistic model of the wollastonite(001) surface in equilibrium with water.

Received: January 7, 2014

Revised: March 17, 2014

Published: March 21, 2014

chemical nature. At ambient conditions, a network of dissociated and associated water molecules forms at the interface. Wollastonite(001) changes its surface stoichiometry in the presence of water because of a metal–proton exchange reaction. Consequently, wollastonite(001), at the water interface, is enriched in Si–OH sites relative to the composition of the bulk material.

2. COMPUTATIONAL METHODS

The present calculations employ density-functional theory (DFT) as implemented in the Vienna ab Initio Simulation Package (VASP).⁴ The electron–ion interaction is treated within the projector-augmented wave (PAW) method.⁵ The valence electron wave functions are expanded into plane waves up to the kinetic energy cutoff of 360 eV. This energy cutoff was found to yield converged structural parameters for bulk wollastonite. The Brillouin zone sampling was performed with $2 \times 2 \times 2$ and $2 \times 2 \times 1$ meshes of Monkhorst–Pack k -points⁶ for the wollastonite bulk and surface calculations, respectively. This was found to ensure an energy convergence better than 0.05 eV. The electron–electron exchange and correlation energy is approximated within the generalized gradient approximation (GGA), using the PW91 functional.⁷ It describes reliably the structure and energetics of hydrogen bonded water monomers.^{8–10}

The optimization of the atomic coordinates (and unit cell size/shape for the bulk materials) was performed via a conjugate gradient technique which utilizes the total energy and the Hellmann–Feynman forces on the atoms (and stresses on the unit cell). The structures were considered to be fully relaxed when the forces on the ions were smaller than 0.01 eV/Å.

We used supercells containing slabs of wollastonite as well as vacuum to describe the surfaces within three-dimensional periodic boundary conditions. In addition to the k -point density and plane-wave cutoff discussed above, the convergence of surface calculations also depends on the thickness of the material slab and the width of the vacuum region between the slabs. The convergence was checked by running a series of test calculations with different slab thicknesses and vacuum regions. Supercells containing two layers of $\text{Ca}_3\text{Si}_3\text{O}_9$ units separated by a vacuum region of approximately 20 Å between the images of the unhydrated surfaces and at least 10 Å between the images of the hydrated surfaces are found to result in converged results. Calculations on reactants and products were performed using equivalent supercells to take advantage of numerical error cancellation. For calculations with charged supercells, we assume a neutralizing background charge.

3. RESULTS AND DISCUSSION

Wollastonite in its most common triclinic phase crystallizes in space group $P\bar{1}$ with the experimental lattice constants $a = 7.94$ Å, $b = 7.32$ Å, $c = 7.07$ Å and six formula units per unit cell.³ The present calculations reproduce these lattice parameters within 3%. As there is no experimental indication for surface reconstructions, we model the (001) surface with a truncated bulk surface. This allows for comparison with previous calculations.^{11,12} On the basis of the calculated equilibrium bulk atomic structure, we model the wollastonite(001) surface as shown in Figure 2 (top view). The ionic relaxation with respect to the bulk positions is marginal and limited to a minor inward relaxation. The chains formed by Si–O tetrahedral

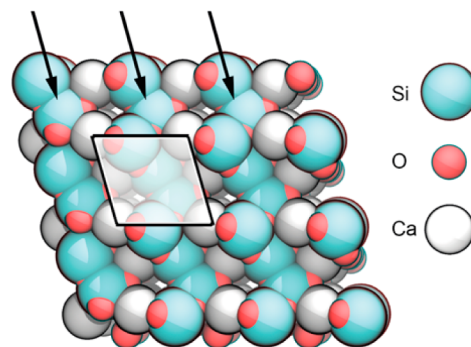


Figure 2. Top view on the clean wollastonite(001) surface. The surface unit cell is highlighted. The arrows indicate the chains formed by Si–O tetrahedra along the crystal b -axis. Gray spheres represent Ca, red spheres represent O, and green spheres represent Si.

groups along the b -axis are clearly recognizable and indicated by arrows in Figure 2. The surface energy is given by

$$\gamma_s = \frac{E_s - E_b}{A} \quad (1)$$

where E_s is the energy of the surface unit of the crystal, E_b is the energy of an equal number of atoms of the bulk crystal, and A is the surface area. The present calculations result in a surface energy of 1.028 J m^{-2} for wollastonite(001). This is somewhat less than obtained in previous atomistic simulations, using force fields: Kundu et al.^{11,12} determined a wollastonite(001) surface energy of 1.36 J m^{-2} . The deviation from the present ab initio result may be accounted to the inherent limitations of force fields with respect to the description of chemical bonds in general and bond-breaking in particular.¹³

In the following, we discuss the adsorption of water on the clean wollastonite(001) surface and first turn to stoichiometric structures of increasing coverage before we discuss non-stoichiometric interfaces and study the influence of the pH value. In the case of stoichiometric adsorption, the water adsorption energy is calculated from the energies of the water-adsorbed surface containing n molecules (E_n), the energy of gas-phase water molecules ($E_{\text{H}_2\text{O}}$), and the energy of the clean slab (E_0) as

$$E_{\text{ads}} = \frac{E_n - E_0 - nE_{\text{H}_2\text{O}}}{n} \quad (2)$$

Figure 3 depicts three favorable adsorption configurations for single water monomers on wollastonite(001). The lowest-energy structure (Figure 3, right) is characterized by water dissociation and leads to a coexistence of Si–OH and Ca–OH groups on the wollastonite(001) surface. The calculated Si–OH, Ca–OH, SiO–H, and CaO–H bond lengths amount to 1.64, 2.21, 0.96, and 0.97 Å, respectively. The Ca–OH groups are placed in the bridge position between two Ca atoms. Both the Ca-adsorbed and the Si-adsorbed OH groups are tilted by 33° with respect to the surface normal.

To better understand the chemical nature of the Si–OH and the Ca–OH bonds, the charge redistribution upon bond formation is investigated. Thus, the difference in charge density of the adsystem and the electron charge of the isolated adgroup and the clean surface is calculated. Figure 4 shows the corresponding results for the Si–OH and Ca–OH groups with charge isolines in a plane defined by the a and c crystal axis that contains the respective hydroxyl group. Charge accumulation

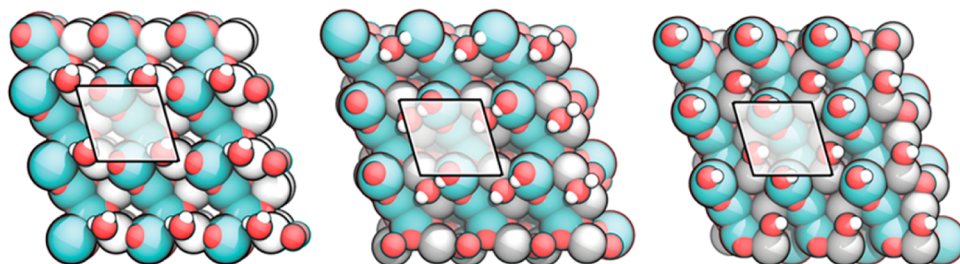


Figure 3. Possible energetically favorable adsorption structures of water monomers on wollastonite(001). Color coding as in Figure 2, with small white spheres representing H.

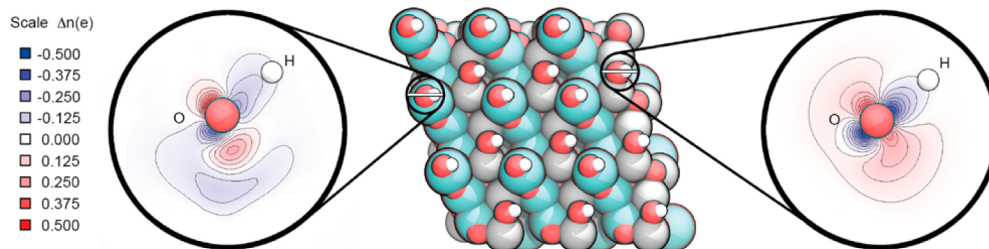


Figure 4. Comparison of the charge redistribution Δn upon coexistence of Si–OH and Ca–OH. The charge isolines in a plane defined by the a and c crystal axis and centered in the Si–OH and Ca–OH group are plotted. Regions where electronic charge is accumulated and depleted are indicated in red and blue, respectively. Color coding as in Figure 3.

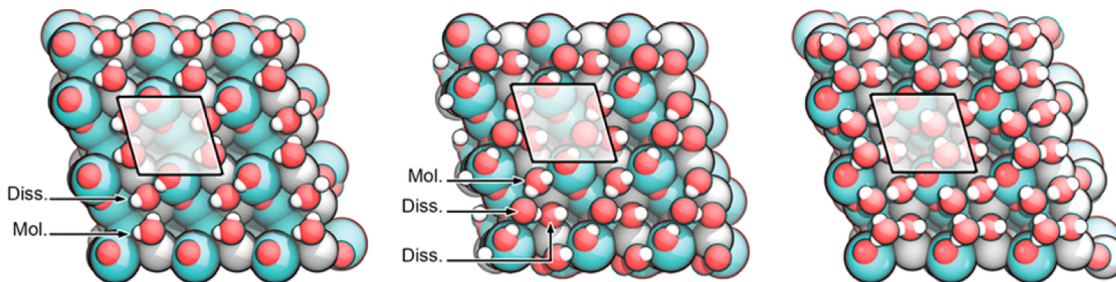


Figure 5. From left to right: Energetically favorable structure of the water dimer, the water monolayer consisting of three water molecules and four water molecules adsorbing on wollastonite(001). Color coding as in Figure 3.

and depletion are indicated in red and blue, respectively. For both the Si–OH and the Ca–OH groups, a weakening of the O–H bond is observed, while additional charge strengthens the bond between the hydroxyl oxygen and the substrate Si or Ca atoms, respectively. The additional charge is mainly O localized in the case of the Si–OH bond, while it is rather delocalized for the Ca–OH group. This charge redistribution does not allow for direct conclusions on the bond strengths. From the total-energy calculations we determine bond strengths of 3.08 eV for Si–OH and 2.50 eV for Ca–OH, respectively. While the hydroxyl groups bond thus stronger to Si than to Ca, the opposite occurs for the hydrogens: The respective bond strengths are 2.61 eV for SiO–H and 3.63 eV for CaO–H, respectively. The difference in the hydrogen bond strengths is larger than 1 eV. From these results we expect the Ca–OH and the Si–OH groups to have more basic and more acidic character, respectively.

Next we turn to higher coverages and adsorb two water monomers per wollastonite(001) surface unit cell. The most favorable structure corresponds to the formation of a water dimer as shown in Figure 5, left. Thereby one of the water monomers adsorbs intact, while one dissociates. The most stable structure for a water monolayer, consisting of three water molecules adsorbed on the wollastonite(001) surface unit cell,

is shown in Figure 5, middle. Thereby water molecules are located in the bridge position between calcium atoms in the energetically favored adsorption configuration formed by alternating dissociated and molecular monomers. Figure 5, right, depicts the energetically most favorable structure consisting of four water molecules adsorbed on the wollastonite(001) surface. Interestingly, the water dissociation rate decreases with increasing coverage: While the ground state of single adsorbed water monomers is found to be dissociated (dissociation rate 100%), no dissociation is found for coverage exceeding the water monolayer (dissociation rate 0%). Higher water coverage was investigated by adsorbing additional molecules on top of the monolayer structure. Thus, up to seven molecules per primitive surface unit cell were considered and various starting configurations were probed. Upon water adsorption, the surface morphology is not substantially modified. In fact, reportable structural modifications are only observed for the vertical distance of the surface calciums. While it amounts to 1.29 Å for the clean, truncated surface, the deeper Ca relaxes toward the surface upon water adsorption. In the structure where four water molecules are adsorbed (Figure 5, right) the spacing between the Ca planes is thus reduced to 0.17 Å.

Figure 6 depicts the adsorption energy E_{ads} as a function of the number of water molecules adsorbed per wollastonite(001)

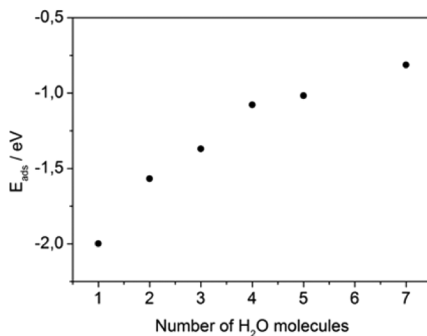


Figure 6. Calculated adsorption energy per water molecule as a function of the number of water molecules within the simulation unit cell.

surface unit cell. The adsorption energy decreases monotonously with increasing water coverage from 2 eV for single water molecule adsorption to 1.4 eV for water monolayer adsorption. This can be explained by the formation of several bonds between admolecule and surface upon dissociative water adsorption for low coverage. The adsorption energies per water molecule fall off for coverage exceeding one monolayer and finally reach the value of water adsorption on ice (1 to 0.6 eV).⁸

However, the adsorption energy alone does not allow a conclusion on the stability of a specific surface structure. Rather, one has to take into account the chemical potentials $\mu(A_i)$ of the surface constituents A_i to compare interfaces with different stoichiometry energetically. The ground state of the surface is determined by the minimum of the thermodynamic grandcanonical potential Ω :

$$\Omega = F - \sum_i \mu(A_i) n_i + q(E_F + E_{\text{VBM}}) \quad (3)$$

where $F = E - TS$ is the surface free energy. Here it is approximated by the total surface energy E assuming similar entropy contributions S for different adsorption configurations. In fact, the differences in vibrational free energy and electronic entropy are typically several orders of magnitude smaller than adsorption energies resulting from chemical bond formation as found in the present case.¹⁴ The last term on the right-hand side accounts for the energy changes due to a possible surface charge q in dependence on the chemical potential of electrons given here by the Fermi level (E_F) measured relative to the valence-band maximum (E_{VBM}) of wollastonite.

If one assumes a neutral and flat, i.e., stoichiometric, wollastonite(001) surface in the presence of pure water, the grandcanonical potential will only depend on the number and chemical potential of the water molecules. Figure 7 (top) shows the resulting phase diagram. Here two important values are indicated. Extreme water-rich conditions are marked by a vertical line denoted $\mu(\text{H}_2\text{O})^{\text{solid}}$. This value corresponds to a wollastonite(001) surface in equilibrium with bulk water approximated here by calculations for ice_{lh}. The corresponding ice calculations reproduce earlier data.⁸ Obviously, for very water-rich conditions, structures not considered here with coverage exceeding two water layers will form. Lower values of $\mu(\text{H}_2\text{O})$ indicate an increasingly dry environment. The zero-temperature calculation for gas-phase water molecules is indicated by another vertical line $\mu(\text{H}_2\text{O})^{\text{gas}}$. The calculations

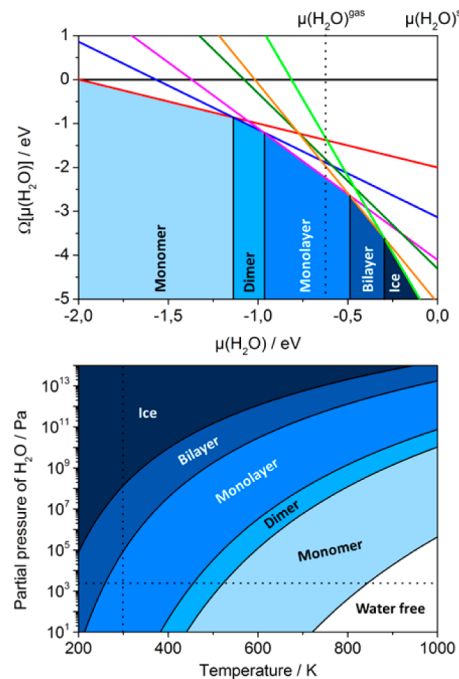


Figure 7. Top: Calculated phase diagram of the water–wollastonite(001) interface as a function of the water chemical potential. Bottom: Calculated phase diagram of the water–wollastonite(001) interface as a function of pressure and temperature (see text).

predict the wollastonite(001) surface to be water covered even for remarkably low water chemical potentials.

The chemical potential can be directly related to experimental conditions. The water chemical potential for surfaces in equilibrium with liquid water is approximated here with the value calculated for water ice, while the pressure- and temperature-dependent modification of the gas-phase water chemical potential $\Delta\mu(\text{H}_2\text{O})$ is estimated within the approximation of a polyatomic ideal gas. Following ref 15, we equate

$$\Delta\mu_{\text{H}_2\text{O}}(p, T) = k_B T \left[\ln\left(\frac{p\lambda^3}{k_B T}\right) - \ln Z_{\text{rot}} - \ln Z_{\text{vib}} \right] \quad (4)$$

where k_B is the Boltzmann constant, p is the pressure, T is the temperature, and λ is the de Broglie thermal wavelength of the water molecule

$$\lambda = \sqrt{\frac{2\pi\hbar^2}{mk_B T}} \quad (5)$$

where m represents the molecular mass.

$$Z_{\text{rot}} = \frac{(2k_B T)^{3/2} (\pi I_1 I_2 I_3)^{1/2}}{\sigma \hbar^3} \quad (6)$$

and

$$Z_{\text{vib}} = \prod_{\alpha} \left[1 - \exp\left(-\frac{\hbar\omega_{\alpha}}{k_B T}\right) \right]^{-1} \quad (7)$$

are the rotational and vibrational partition functions, respectively. For the evaluation, we use the experimental momenta of inertia I_i and vibrational frequencies ω_{α} of the water molecule. The geometrical parameter $\sigma = 2$ takes the symmetry of the water molecule into account.

Figure 7 (bottom) shows the resulting phase diagram as a function of water partial pressure and temperature. Dotted lines indicate the ambient conditions. At ambient conditions, the wollastonite(001) surface is water monolayer covered, and only for high temperatures in excess of 800 K does the water desorb.

Next we consider the case where the surface is in equilibrium with bulk water but vary the pH value. For computational reasons, we are thereby limited to a water thin film of monolayer thickness adsorbed on wollastonite(001). We study the stability of various stoichiometries as well as surfaces with varying surface charge. In the following we use a notation where W_{xyz} refers to a structure that has x Ca atoms less and y additional hydrogen atoms adsorbed per unit cell with respect to a stoichiometric surface; z denotes the surface charge.

To assess the stability of the numerous model structures that were probed again, the thermodynamic grandcanonical potential was investigated. However, now additional degrees of freedom enter: Not only the number of water molecules but also the numbers of surface Ca and O atoms as well as H and electrons will not be the same anymore for different structures. The respective chemical potentials are not independent from each other:

(i) The sum of the chemical potentials of the surface constituents Ca and O is here assumed to equal the chemical potential of the CaO bulk

$$\mu(\text{CaO})_{\text{bulk}} = \mu(\text{Ca}) + \mu(\text{O}) \quad (8)$$

(ii) The chemical potentials of oxygen and hydrogen are related to the chemical potential of water

$$\mu(\text{H}_2\text{O}) = 2\mu(\text{H}) + \mu(\text{O}) \quad (9)$$

(iii) The chemical potential of hydrogen is related to the chemical potentials of electrons and protons

$$\mu(\text{H}) = \mu(\text{e}^-) + \mu(\text{H}^+) \quad (10)$$

(iv) The chemical potential of protons, in turn, is related to the pH value by

$$\mu(\text{H}^+) = \mu_0 - \text{pH} \times 0.05918 \text{ eV} \quad (11)$$

where μ_0 contains the proton solvation enthalpy in water, see, e.g., ref 16. The pH value determines the chemical potential of protons via eq 11, that directly enters the grand canonical potential given by eq 3.⁹ For the present calculations, we assume the chemical potential of electrons, i.e., the Fermi level, to be fixed at the valence-band maximum (E_{VBM}) of the ideal wollastonite crystal. The latter is calculated from the energy difference between a slightly charged ($q = 0.001 \text{ e}$) and neutral unit cell

$$E_{\text{VBM}} = \frac{E_{\text{bulk}}^0 - E_{\text{bulk}}^{0.001}}{0.001} \quad (12)$$

If we again approximate the water chemical potential by the respective value for bulk ice $\mu(\text{H}_2\text{O})^{\text{solid}}$, the stability of the various structures can be directly compared for a given pH value. A word of caution is certainly in order with respect to the phase diagram calculated based upon these approximations: Apart from slight deviations of the chemical potentials due to chemical reservoirs that differ from the assumptions made here, temperature effects are neglected and the necessarily limited number of structures and charge states that can be considered will impair its predictive power. In particular the limitation to structures that have the periodicity of the wollastonite (1×1)

surface unit cell represents a severe limitation. Still, we expect a meaningful description of the chemical trend.

The energetically most relevant structures are shown in Figure 8, and the resulting phase diagram is shown in Figure 9.

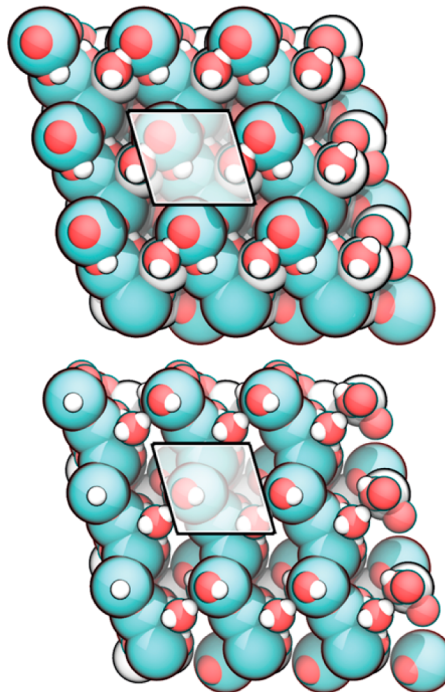


Figure 8. Energetically favorable interface structures W120 (top) and W240 (bottom). Color coding as in Figure 3.

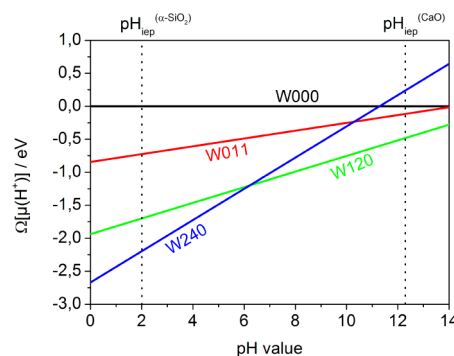


Figure 9. Calculated phase diagram of the wollastonite(001)-water interface as a function of the pH value. For clarity, only the most favorable structures are shown.

Among the structures investigated, we find W120 stable for neutral to basic conditions, while W240 is favored for more acidic water. The present results show that the wollastonite(001) surface in contact with neutral and moderately acidic aqueous solution is enriched in Si-OH sites relative to the composition of the bulk mineral (Figure 8 (bottom), W240 in Figure 9).



It occurs already at a basic pH value (Figure 8 (top), W120 in Figure 9). The surface of wollastonite(001) in contact with neutral and moderately acidic aqueous solution is enriched in Si-OH sites relative to the composition of the bulk mineral (Figure 8 (bottom), W240 in Figure 9).

Oelkers et al.¹⁷ investigated the metal–proton exchange reaction on different minerals and concluded that the number of protons consumed by each exchange reaction is mineral specific. The number of protons consumed by the exchange of Ca from wollastonite surfaces was found to be less than 2, suggesting that fewer protons are consumed by the removal of Ca than required to compensate for the loss of charge. Casey et al. reported repolymerization of Si–OH sites on the wollastonite surface during its leaching to be a possible reason for this.¹⁸ Electrokinetic measurements yielded isoelectric points of 2.0, 2.6, and 12.3 for SiO_2 , wollastonite, and CaO.¹⁷ This is again consistent with the predominance of Si–OH sites at the water–wollastonite(001) interface. In a very recent article, Ebbert et al. have proved the formation of a C-S-H phase on native oxide covered silicon wafer.¹⁹ The total thickness of the C-S-H phase was determined by X-ray photoelectron spectroscopy (XPS) to be 3 nm. This preparation technology will provide reproducible samples for further investigations in near future.

Deposition of thin films and grafting of organic molecules on mineral surfaces, particularly oxide surfaces, are widely studied as means of passivation and functionalization for a variety of applications. However, organic functionalization of minerals is challenging, as the currently used molecules (silanes) do not form layers that are stable in aqueous environments and present challenges (homocondensation) during the grafting process. Indeed, in contrast to most of the metal–phosphonic acid bonds (e.g., Al–O–P), the Si–O–Si bond is sensitive toward hydrolysis, particularly in basic solutions.^{20,21} The modification of Si–OH-enriched mineral surfaces with metal oxides may represent an attractive alternative because strong bonds can be established between metal oxides and relevant molecules (silanes, carbonic acids, phosphonic acids). Our results suggest wet chemical processing following the paradigm of the metal–proton exchange reaction as an inexpensive and technologically very attractive method for depositing an ultrathin layer of metal oxide/hydroxide groups.

4. CONCLUSIONS

Using density-functional theory it is shown that (i) single water monomers adsorb dissociatively on wollastonite(001) and lead to the coexistence of Si–OH and Ca–OH groups on the surface. Our calculations predict the Si–OH groups to be more acidic than the Ca–OH groups. (ii) The rate of dissociation as well as the adsorption energy decreases with increasing water coverage. (iii) At ambient conditions, a network of dissociated and associated water molecules is formed at the interface. (iv) The mineral changes its surface stoichiometry in the presence of water, already a basic pH value due to metal–proton exchange. Consequently, wollastonite(001) at the water–mineral interface is enriched in Si–OH sites relative to the composition of the bulk material. Our findings suggest exploiting the metal–proton exchange reaction to drive metals back to the mineral surface and to use metal oxide activation²² of Si–OH for organic functionalization.

AUTHOR INFORMATION

Corresponding Author

*Phone: +49 721 608-23374. E-mail: peter.thissen@kit.edu.

Notes

The authors declare no competing financial interest.

ACKNOWLEDGMENTS

We thank the DFG for financial support. The Texas Advanced Computing Center (TACC) is acknowledged for computational resources.

REFERENCES

- (1) Richardson, I. G. The calcium silicate hydrates. *Cement Concrete Res.* **2008**, *38* (2), 137–158.
- (2) Richardson, I. G. Tobermorite/jennite- and tobermorite/calcium hydroxide-based models for the structure of C-S-H: applicability to hardened pastes of tricalcium silicate, beta-dicalcium silicate, Portland cement, and blends of Portland cement with blast-furnace slag, metakaolin, or silica fume. *Cement Concrete Res.* **2004**, *34* (9), 1733–1777.
- (3) Ohashi, Y. Polysynthetically-twinned structures of enstatite and wollastonite. *Phys. Chem. Miner.* **1984**, *10* (5), 217–229.
- (4) Kresse, G.; Furthmüller, J. Efficiency of ab-initio total energy calculations for metals and semiconductors using a plane-wave basis set. *Comp. Mater. Sci.* **1996**, *6* (1), 15–50.
- (5) Kresse, G.; Joubert, D. From ultrasoft pseudopotentials to the projector augmented-wave method. *Phys. Rev. B* **1999**, *59* (3), 1758–1775.
- (6) Monkhorst, H. J.; Pack, J. D. Special points for Brillouin-zone integrations. *Phys. Rev. B* **1976**, *13* (12), 5188–5192.
- (7) Perdew, J. P.; Chevary, J. A.; Vosko, S. H.; Jackson, K. A.; Pederson, M. R.; Singh, D. J.; Fiolhais, C. Atoms, molecules, solids, and surfaces: Applications of the generalized gradient approximation for exchange and correlation. *Phys. Rev. B* **1992**, *46* (11), 6671–6687.
- (8) Thierfelder, C.; Hermann, A.; Schwerdtfeger, P.; Schmidt, W. G. Strongly bonded water monomers on the ice Ih basal plane: Density-functional calculations. *Phys. Rev. B* **2006**, *74* (4), 045422.
- (9) Thissen, P.; Thissen, V.; Wippermann, S.; Chabal, Y. J.; Grundmeier, G.; Schmidt, W. G. pH-dependent structure and energetics of $\text{H}_2\text{O}/\text{MgO}(100)$. *Surf. Sci.* **2012**, *606* (11–12), 902–907.
- (10) Thissen, P.; Grundmeier, G.; Wippermann, S.; Schmidt, W. G. Water adsorption on the alpha- $\text{Al}_2\text{O}_3(0001)$ surface. *Phys. Rev. B* **2009**, *80* (24).
- (11) Kundu, T. K.; Rao, K. H.; Parker, S. C. Atomistic simulation of the surface structure of wollastonite and adsorption phenomena relevant to flotation. *Int. J. Miner. Process.* **2003**, *72* (1–4), 111–127.
- (12) Kundu, T. K.; Rao, K. H.; Parker, S. C. Atomistic simulation of the surface structure of wollastonite. *J. Chem. Phys. Lett.* **2003**, *377* (1–2), 81–92.
- (13) de Leeuw, N. H.; Purton, J. A.; Parker, S. C.; Watson, G. W.; Kresse, G. Density functional theory calculations of adsorption of water at calcium oxide and calcium fluoride surfaces. *Surf. Sci.* **2000**, *452* (1–3), 9–19.
- (14) Wippermann, S.; Schmidt, W. G. Entropy explains metal-insulator transition of the Si(111)-In nanowire array. *Phys. Rev. Lett.* **2010**, *105* (12).
- (15) Landau, L. D.; Lifshitz, E. M. *Lehrbuch der Theoretischen Physik*; Akademie-Verlag: Berlin, 1987; Vol. 5, pp 125–142.
- (16) Himmel, D.; Goll, S. K.; Leito, I.; Krossing, I. A unified pH scale for all phases. *Angew. Chem., Int. Ed.* **2010**, *49* (38), 6885–6888.
- (17) Oelkers, E. H.; Golubov, S. V.; Chairat, C.; Pokrovsky, O. S.; Schott, J. The surface chemistry of multi-oxide silicates. *Geochim. Cosmochim. Acta* **2009**, *73* (16), 4617–4634.
- (18) Casey, W. H.; Westrich, H. R.; Banfield, J. F.; Ferruzzi, G.; Arnold, G. W. Leaching and reconstruction at the surfaces of dissolving chain-silicate minerals. *Nature* **1993**, *366* (6452), 253–256.
- (19) Ebbert, C.; Grundmeier, G.; Buitkamp, N.; Kröger, A.; Messerschmidt, F.; Thissen, P. Toward a microscopic understanding of the calcium–silicate–hydrates/water interface. *App. Surf. Sci.* **2014**, *290*, 207–214.
- (20) Haller, I. Covalently attached organic monolayers on semiconductor surfaces. *J. Am. Chem. Soc.* **1978**, *100* (26), 8050–8055.

- (21) Pasternack, R. M.; Rivillon Amy, S.; Chabal, Y. J. Attachment of 3-(aminopropyl)triethoxysilane on silicon oxide surfaces: Dependence on solution temperature. *Langmuir* **2008**, *24* (22), 12963–12971.
- (22) Thissen, P.; Vega, A.; Peixoto, T.; Chabal, Y. J. Controlled, low-coverage metal oxide activation of silicon for organic functionalization: Unraveling the phosphonate bond. *Langmuir* **2012**, *28* (50), 17494–17505.